Apoptosis
https://doi.org/10.1007/s10495-019-01541-z

Endothelin-1-mediated cerebral ischemia in mice: early cellular events and the role of caspase-3

Chesarahmia Dojo Soeandy[1] · Faraz Salmasi[1] · Maya Latif[1] · Andrew J. Elia[2,3] · Nan Ji Suo[1] · Jeffrey T. Henderson[1]

Abstract

Over the past 30 years a number of animal models of cerebral ischemic injury have been developed. Middle cerebral artery occlusion (MCAO) in particular reproduces both ischemic and reperfusion elements and is widely utilized as a model of ischemic stroke in rodents. However substantial variability exists in this model even in clonal inbred mice due to stochastic elements of the cerebral vasculature. Models such as MCAO thus exhibit significant irreducible variabilities with respect to their zone of injury as well as inducing a sizable volume of injury to the cerebrum with damage to sub-cortical structures, conditions not typically seen for the majority of human clinical strokes. An alternative model utilizes endothelin-1 application focally to cerebral vasculature, resulting in an ischemic reperfusion injury which more closely mimics that seen in human clinical stroke. In order to further define this model we demonstrate that intra-cortical administration of ET-1 results in a highly reproducible pattern of tissue injury which is limited to the cerebral cortex, characterizing the early cellular and molecular events which occur during the first 24 h post-injury. In addition we demonstrate that caspase-3 is both necessary and sufficient to regulate a majority of cortical cell death observed during this period. The enhanced survival effects seen upon genetic deletion of caspase-3 appear to arise as a result of direct modification of cell autonomous PCD signaling as opposed to secondary effectors such as granulocyte infiltration or microglia activation. Taken together these findings detail the early mechanistic features regulating endothelin-1-mediated ischemic injury.

Keywords Murine models of stroke · Gene knockout · Programmed cell death · MCAO · Apoptosis · Endothelin-1

Introduction

Stroke remains a leading cause of long-term disability and death affecting fifteen million people worldwide yearly [1]. These can be broadly divided into two major forms: ischemic and hemorrhagic strokes. Ischemic strokes occur as a result of obstruction of cerebral blood flow whereas haemorrhagic strokes arise as a consequence of leakage or rupture of cerebral vasculature. Greater than 85% of clinical strokes are observed to be of the ischemic type [2, 3]. Neurologic response to stroke is complex involving both cell extrinsic (release of inflammatory mediators promoting astrocytic and microglial reorganization, infiltration and proliferation of neighboring cells, induction of phagocytosis etc.) and intrinsic components (excessive glutamate release; calcium/sodium influx with cell swelling, depletion of cellular ATP stores, rise of intracellular reactive oxygen and nitrogen species; activation of HIF-1 alpha and programmed cell death signaling pathways) in response to tissue hypoxia. Histologically, cortical ischemic injury demonstrates the presence of two morphologically distinct forms of cell death in neurons: a necrotic isoform prevalent in regions exposed to more prolonged and severe hypoxic insult, and less severely affected (penumbral) regions of injury demonstrating features of apoptosis [4]. With respect to apoptotic signaling two key pathways have been described termed the extrinsic and intrinsic apoptotic pathways [5, 6]. While the former is stimulated through the activation of TNFR, Fas, TRAIL

✉ Jeffrey T. Henderson
jeff.henderson@utoronto.ca

[1] Department of Pharmaceutical Sciences, University of Toronto, 144 College St. Rm 962, Toronto, ON M5S 3M2, Canada

[2] Princess Margaret Cancer Center, University Health Network, 610 University Avenue Rm 7-323, Toronto, ON M5G 2C1, Canada

[3] Department of Medical Biophysics, University of Toronto, 101 College Street Rm 15-701, Toronto, ON M5G 1L7, Canada

Published online: 09 May 2019

and Toll-like receptors, the latter is dominantly regulated by the balance of pro- (Bax/Bak) and anti- (Bcl2/Bcl-xl) Bcl-2 interactions occurring along the mitochondrial outer membrane [6, 7]. These signaling pathways are known to intersect at the level of the mitochondria where release of holo-cytochrome C from the mitochondrial intermembranous space promotes formation of the apoptosome (minimally comprised of cytochrome C, Apaf-1 and dATP) [8]. Apoptosome formation promotes the autocatalytic activation of caspase-9, in turn promoting the proteolytic activation of executioner caspases-3, −6 and −7 [9–11]. Activation of these caspases initiates the final (irreversible) phase of programmed cell death which plays a key role in the induction of cell death through cleavage of a large number of structural and enzymatic targets including actin, poly-ADP ribose polymerase (PARP), caspase-activated DNase (CAD), focal adhesion kinase (FAK), paxillin, lamin, protein kinase C (PKC), and fodrin [12–14].

Clinical treatments for ischemic stroke have focused largely on supportive measures such as the reestablishment of vascular perfusion via administration of thrombolytics such as tissue plasminogen rather than direct inhibition of neuronal death [15]. Despite the fact that a number of candidate neuroprotective drugs have been tested in animal stroke models over the last several decades, few have successfully completed stage III clinical trials [16–18]. While in some respects this reflects inherent limitations of these systems to duplicate aspects of human physiology and cell biology (immune function, tissue expression of cytokines and their receptors, gene expression and regulation, features of drug distribution and anatomy) [16, 18, 19], in acute stroke research this failure has also been suggested to reflect underlying deficiencies in the very nature of the models most often utilized to evaluate such treatments [16, 20]. Though substantial progress has been made over the past several decades in understanding mechanisms of hypoxic injury; features of a number of ischemic models utilized in rodents deviate significantly from forms of injury most commonly seen in humans [20]. Even among rodent models reproducing both ischemic *and* reperfusion components of hypoxic injury such as middle cerebral artery occlusion (MCAO), several significant differences exist between the features of this model and conditions most commonly observed clinically during cortical ischemia. Among these is both the extent and neurologic structures affected during MCAO, which typically ranges from 21 to 45% of the affected hemisphere and induces injury in a variety of cortical and subcortical structures [20]. By contrast the majority of human clinical strokes affect 2–14% of the neocortex and are limited to the cortex and typically involve end-arteriolar or small vessel hypofusion [3, 20–23]. An additional confounding variable is the stochastic properties of middle cerebral artery development. As a result, significant variability in innervation territory of the middle cerebral artery is observed, even in clonal inbred lines of mice [24]. This is also true with respect to patterns of individual collateral circulation. Additionally this technique requires intra-arterial entry into the carotid artery to occlude the middle cerebral artery, creating an additional source of potential variability with respect to bleeding and the extent of localized occlusion between animals; critical factor to stroke outcome [25]. Such model-based deviations create significant barriers to clear and consistent interpretation with respect to the extent and totality of hypoxic injury and may underlie the above difficulties in clinical translation.

Use of a physiologic vasoconstrictive end-arteriolar ischemic/reperfusion model would address many of the above problems by precluding vascular entry and allow stereotactic control of the pattern of ischemic injury. One such model involves the intra-cortical application of endothelin-1 (ET-1), a vasoactive peptide which is released during human ischemic stroke [26]. Time course analysis of endothelin-1 on reduction of cerebral blood flow demonstrates that it induces reversible ischemic hypofusion for periods of greater than 1 h [27, 28]. While this approach has successfully been used to induce cortical ischemia in rats [29–31], results in murine strains have been mixed [28, 32–34]. In the current study we characterized cellular and molecular responses to intra-cortical application of ET-1 in several murine strains including those lacking caspase-3. Our results demonstrate that ET-1 can safely and reproducibly generate well-defined regions of cortical ischemic insult in the murine cortex which more closely mimic conditions seen for the majority of human clinical strokes. Within the cortex several distinct forms of neuronal cell death are observed 24 h post-injury, with loss of caspase-3 reducing lesion volumes by approximately 60%.

Materials and methods

Animals

Animals were housed under standard conditions with a 12 h light/dark cycle and ad libitum access to standard rodent chow and water. Procedures performed were done in compliance with standards set by the Local Animal Care Committee and the University of Toronto, in accordance with the requirements under Ontario's Animal for Research Act and the federal Canadian Council on Animal Care. Caspase-3 heterozygous and null mice were generated as previously described [35]. CD1 and C57BL/6J utilized were 2–4 months of age and 21–28 grams in weight at the time of surgery.

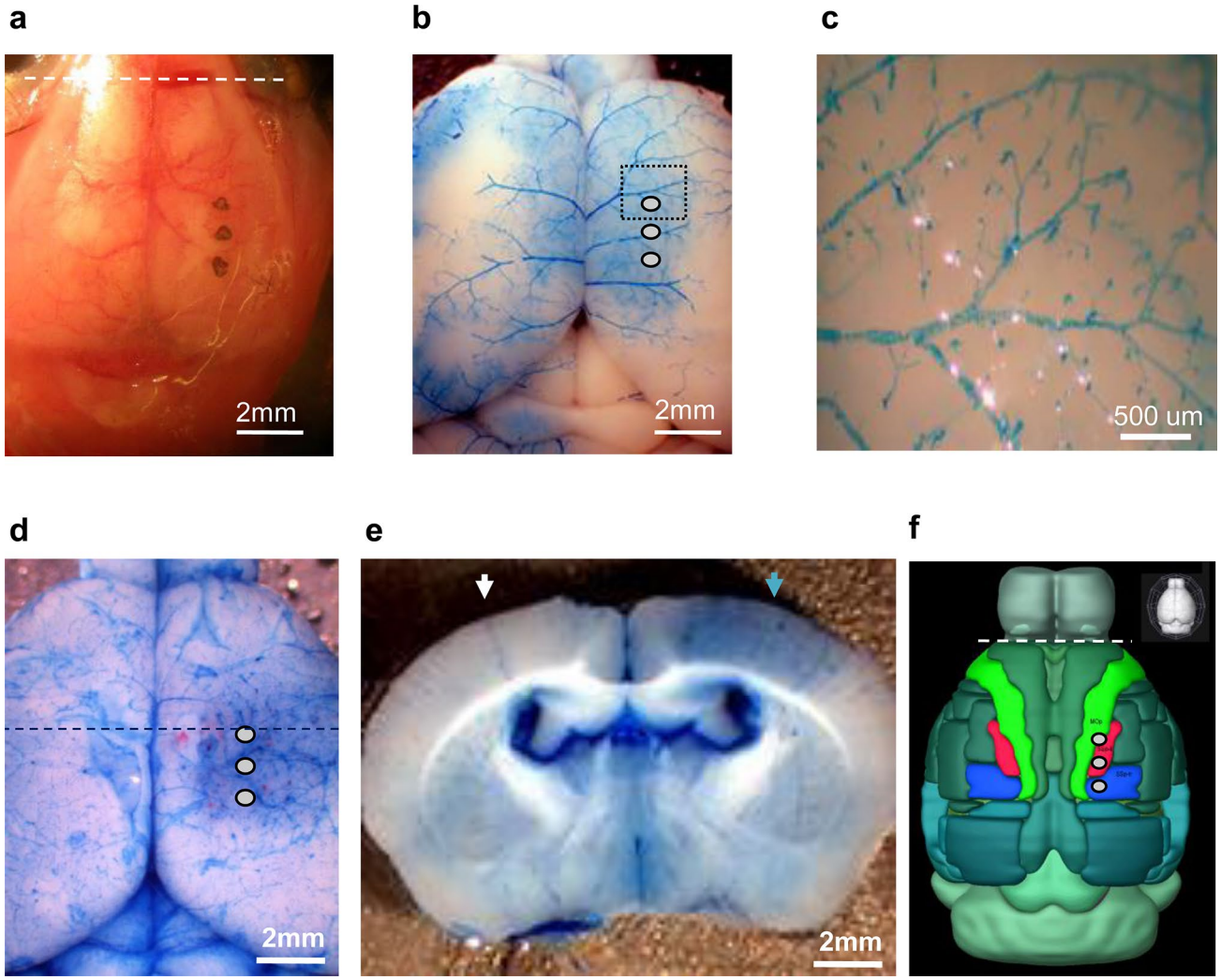

Fig. 1 Induction of cortical ischemic-reperfusion injury using endothelin-1. **a** Dorsal overview of murine skull highlighting relative positions of stereotactic infusion sites for endothelin-1 within the murine cortex. Dotted line indicates dorsal extent of the rostral rhinal vein for reference. **b** Infusion cast demonstrating the pattern of arterial perfusion within the dorsal cortex following unilateral dye injection of the left common carotid artery. Relative position of endothelin-1 injection sites are indicated (circle). Relative position of details shown in (**c**) is also highlighted (square). **c** Higher magnification view of the dorsal cortex illustrating pattern of penetration of short and long cortical arterioles. **d** Example of trypan blue (TB) extravasation within cerebral vasculature 24 h following endothelin-1 injection (injection sites indicated). Dashed line indicates the level of the coronal view shown in (**e**). **e** Coronal view highligthing relative levels of TB extravasation from pial arterioles within the dorsal cortex (white arrow: contralateral to injury, blue arrow: ipsilateral). **f** Schematic illustrating relative position of functional cortical domains relative to the endothelin-1 injection. Highlighted domains delineate primary motor (green) and primary somatosensory areas of the lower limb (red) and trunk (blue) (Allen Mouse Brain Atlas) [67] (Color figure online)

Stereotactic injections

Wild-type (WT) CD1, C57BL/6J or caspase-3 null mice were weighed and anaesthetized with an appropriate volume of 2.5% Avertin with temperature monitoring. Experimenter was blinded with respect to animal genotype. At the start of surgery, Ketoprofen (0.05 mg/10 g, s.c.) was injected subcutaneously as an analgesic. Overlying dermal hair was removed from the dorsal skull over a one centimeter area, the skin then sterilized and a 0.8 cm incision performed along the dorsal midline of the skull between the lambda and bregma sutures. Mice were then placed into a standard Cunningham mouse stereotactic frame with controlled body temperature support. Stereotactic sites for cortical infusions were determined using a strain-specific three dimensional atlas as previously described [36]. Infusions consisted of three sites which were 2.0 mm lateral to the midline (mediolateral-ML) and 0.0, + 1.0 and + 2.0 mm relative to the bregma (anteroposterior-AP, Fig. 1), affecting arterioles originating from the anterior cerebral artery via the azygous

pericallosal, anterior and middle internal frontal arteries as previously described [37]. Cannula depth was +1.2 mm relative to the brain surface (dorsoventral- DV). At each site a 250 µm diameter hole was drilled in the skull and 400 nL of 1 µg/µL endothelin-1 (160 pmol, R&D systems catalogue # 1160) or vehicle control infused through a pulled borosilicate glass capillary of O.D. 100 µm. Following endothelin-1 delivery, cannula was held in place for 2 min to allow for fluid equalization prior to removal and the overlying dermis closed with 6.0 polyurethane sutures. Procedures were completed over a period of 30 min. Animals were then placed in a recovery cage with temperature monitoring at 37 °C for 15 min prior to their anesthetic recovery cage 25 °C.

TTC staining, tissue sectioning and electron microscopy

TTC staining

At the indicated times tissues were harvested and prepared for analysis. To identify regions of inhibited cellular respiration 2, 3, 5-Triphenyl tetrazolium chloride (TTC) staining was performed immediately following removal of the brain and dissection into 2 mm cortical slices. Sections were stained in 1% pre-warmed TTC (Sigma #T8877) in phosphate buffered saline, pH 7.4 for 10 min at 37 °C as previously described [38, 39]. Sections were then washed and fixed in 4% para-formaldehyde in PBS overnight at 4 °C and imaged.

Tissue sectioning

Samples for histology/immunohistochemistry were fixed in 4% para-formaldehyde in phosphate buffered saline at pH 7.4 for 30 min at room temperature with agitation followed by 4 °C overnight. Tissues were then dehydrated through a standard automated ethanol/xylene/wax series using a Tissue Tek VIP 3000 processor and embedded in paraffin. Following trimming, sample blocks were sectioned at 7 µm. For each of the experimental condition examined samples were sectioned, in either horizontal or coronal planes through a minimum of 2 mm of surrounding tissue at an interval of 147 µm. Following de-waxing and rehydration samples were processed for immune- or histochemistry as indicated below.

Electron microscopy

Samples for electron microscopy were fixed in 2% glutaraldehyde prepared in 100 mM cacodylate buffer, pH 7.4 overnight at 4 °C. Samples were then treated with 1% osmium tetroxide and embedded in Spurr resin as previously described in Sakai et al. [40]. Tissue blocks were then sectioned at 70 nm onto Formvar coated grids and imaged using a Phillips CM 100 electron microscope at the magnification indicated.

Histochemistry, immunohistochemistry and TUNEL assay

For thionin staining, sections were dewaxed and rehydrated in a series of xylene/ethanol/water baths prior to staining with 0.1% acidified Thionin for 10 s followed by dehydration and mounting with Permount (Fisher). For peroxidase immunohistochemistry, sections were re-hydrated as above and incubated in 0.3% hydrogen peroxide for 15 min at room temperature in order to destroy any endogenous peroxidase activity. Where indicated antigen retrieval was performed in a buffer of 10 mM sodium citrate, pH 6.0 at 100 °C for 10 min using a pressure cooker. Sections were incubated in primary antisera (activated-caspase 3 at 1:1000- Cell signalling catalogue # 9661s; activated-caspase 7 at 1:50-Cell signalling catalogue # 9491s; CD11b at 1:2000—Abcam ab133357; F4/80 at 1:200—Bio-Rad MCA497GAR) in histoblock solution (containing 3% BSA, 20 mM $MgCl_2$, 0.3% tween 20 in 10 mM PBS pH 7.4) with the addition of 0.2% Triton-X-100 and 5% goat serum overnight at 4 °C. Sections were washed once for 5 min in 0.03% PBS-T and 3 × 5 min in PBS and incubated with goat anti-rabbit or anti-mouse biotinylated secondary antisera (1:400-) in PBS solution 0.2% Triton-X-100 for 1 h at room temperature. After washing once for 5 min in 0.03% PBS-T and 3 × 5 min in PBS, sections were incubated in avidin-HRP (1:100 ABC Vectastain Elite kit, Vector labs) according to manufacturer's instructions for 1 h. Sections were then washed and developed using 3,3-diaminobenzidine (DAB peroxidase substrate kit, Vector labs) according to manufacturer's instructions (0.05% DAB, 0.015% H_2O_2 in 10 mM PBS pH 7.5). This was followed by a 5-min counter-stain using hematoxylin with subsequent dehydration and mounting using Permount (Fisher). TUNEL analysis was performed following permeabilization of tissue with 20 µg/ml Proteinase K (Bioshop, PRK403.100) in 10 mM Tris pH 7.5 for 17 min in 37 °C water bath. Slides were then rinsed 3 × 5 min in PBS and FITC-labeled TUNEL reagent applied for 1.5 h according to the manufacturer's instructions (Roche Diagnostics catalogue # 11684795910). Slides were subsequently washed 3x 5 min in PBS. Where indicated sections were incubated in primary antisera (NeuN at 1:200- Chemicon catalogue # MAB377; GFAP at 1:400- Dako catalogue # Z0334) in 10 mM PBS pH 7.4 containing 0.3% tween 20, 5% goat serum overnight at 4 °C. Sections were washed 3 × 5 min in 0.3% PBS-T with 5% goat serum and incubated with goat anti-mouse (1:100-) or anti-rabbit (1:200) TRITC-labeled fluorescent secondary antisera in PBS containing 0.3% tween 20 for 2 h at 4 °C. Slides were then washed 3

× 5 min in PBS with a final wash in 10 mM Tris HCl pH 7.5 for 5 min prior to mounting and imaging.

PCR

Caspase-3 status was determined by PCR amplification using Terra PCR polymerase in a QIAxcel Advanced System analyzed using ScreenGel Software. PCR primers utilized were as follows: WT-Forward: CT CAG GTG CCA GTC ATC CAT, WT-Reverse: CCA TAC ATG GGA GCA AGT CAG, Caspase-3 null-Forward: TCT ATT TGT TCA GTG TTG GAT, Caspase-3 null-Reverse: TCA TTC TCA GTA TTG TTT TGC, with wild-type (WT) primers generating a band of 450 bp, and caspase-3 mutants 850 bp.

Image analysis and statistics

Thionin and DAB-stained sections were digitally scanned using a Hamamatsu Nanozoomer 2.0 HT scanner and recorded at native resolutions of 40×. Region of interest (ROI) measurements were done using NanoZoomer's Digital Pathology software. Total lesion volumes were determined from sections obtained at intervals of 147 µm multiplied by the lesion area observed for each slide. Image quantification was blinded with respect to treatment group. Fluorescent images were recorded at native resolutions of 4× and 10× using on a Nikon E1000R motorized microscope equipped with standard DAPI, FITC, TRITC and Cy5/DiD excitation/emission filters. Fluorescent cell counts were determined from Nikon E1000R gray-scaled images following group-wise adjustment using Adobe Photoshop. For statistical comparison of 2 groups, Welch's t-test (unpaired, two tailed t-test with assumption of unequal variance) was used to determine levels of significance between groups with a minimum level of $p < 0.05$. For comparison of 3 groups, a one-way ANOVA followed by Tukey's post hoc was done to determine levels of significance between groups with a minimum level of $p < 0.05$.

Results

Stereotactic injection of endothelin-1 results in a highly reproducible lesion within the murine cerebral cortex

Endothelin-1 is a 21 amino acid vasoactive peptide produced naturally during cortical stroke that has previously been used to induce ischemic injury. Several dosing paradigms were examined in order to determine the optimal conditions by which we could reproducibly confine the locus of injury to the cortex while minimizing damage to subcortical and associated structures. This ultimately resulted in the infusion of 400 nL of 1 µg/µL human endothelin-1 (160 pmol) into the murine cerebral cortex at each of the 3 sites via a pulled borosilicate capillary (I.D. ~ 80 µm) at the coordinates described in materials and methods and shown in Fig. 1a–f. Distribution of local arterial anatomy is shown in Fig. 1b, c following unilateral dye injection of the left common carotid artery. Infusion of endothelin-1 at these sites induces vasoconstriction of arterioles arising from the anterior cerebral artery via the azygous pericallosal, anterior and middle internal frontal arteries as previously discussed. The detrimental consequence of this induced ischemic/reperfusion injury is shown in Fig. 1d, e, where 24 h following endothelin-1 treatment trypan blue extravasation into surrounding brain parenchyma is markedly enhanced in treatment zones compared to the contralateral cortex (Fig. 1e, blue versus white arrows). Cortical motor and somatosensory domains affected by treatment are indicated in Fig. 1f. The nature and limits of the region of injury following injection of endothelin-1 is shown in Fig. 2. As shown in the horizontal sections in Fig. 2a, b, insertion of the borosilicate cannula with injection of 400 nL vehicle induces a modest level of physical injury at 24 h. Both thionin (Fig. 2a) and TUNEL (Fig. 2b) staining demonstrates cellular injury which is confined to the proximal area of cannula insertion. Figure 2c, d demonstrates that the level of cortical vasoconstrictive injury is significantly expanded in the presence of endothelin-1 as per both thionin and TUNEL. To investigate the extent of cortical injury induced by endothelin-1, murine cortices were also sectioned in the coronal plane throughout the region of injury. As shown in Fig. 2e–h, injection of vehicle resulted in focal injury throughout the laminar cortex which is substantially expanded in the presence of endothelin-1. Consistent with this, Triphenyl tetrazolium chloride (TTC) staining performed 24 h following endothelin-1 injection (Fig. 2i–k) demarcates regions of inhibited cellular respiration ipsilateral but not contralateral to the site of treatment. As further detailed by both thionin (Fig. 2e, g) and TUNEL (Fig. 2f, h) staining this level of injury extends throughout the full thickness of the cortex but does not extend to subcortical structures.

Cellular features of endothelin-1 mediated cortical injury

To confirm whether TUNEL positive cells seen in the region of injury in the cortex were apoptotic in nature, we examined these tissues for evidence of caspase activation. Analysis of the cellular distribution of activated caspase-3 demonstrated the presence of positively stained cells in both coronal (orange arrowheads, Fig. 3a) and horizontal (Fig. 3b) planes. Notably there was a tendency for greater numbers of activated caspase-3 positive cells more distal to the site of injury (150–350 µm) (Fig. 3b) compared to

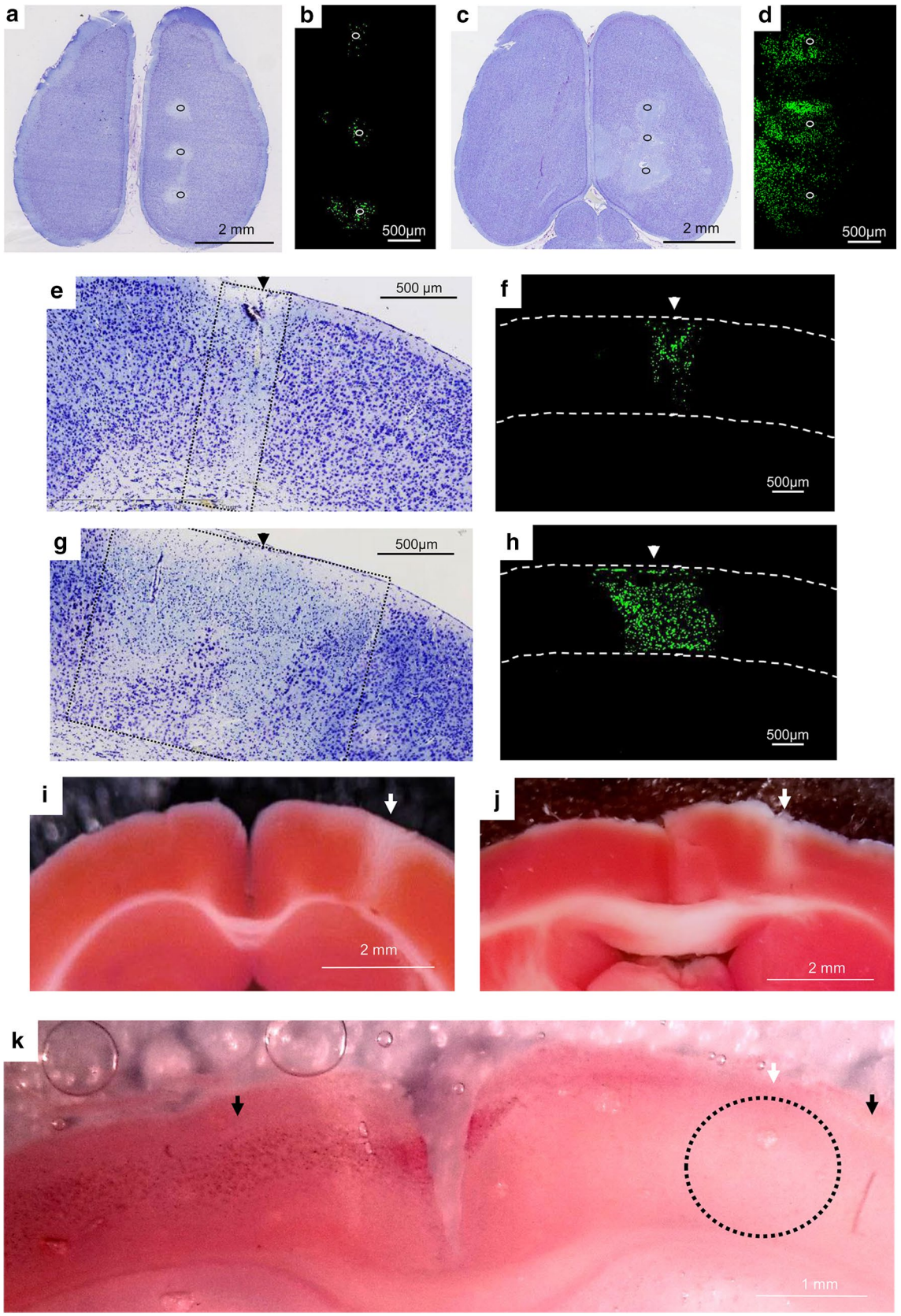
a
2 mm
b
500μm
c
2 mm
d
500μm
e
500 μm
f
500μm
g
500μm
h
500μm
i
2 mm
j
2 mm
k
1 mm

◂**Fig. 2** Stereotactic injection of endothelin-1 induces a reproducible pattern of ischemic injury in the dorsal cortex. **a–d** Horizontal overviews of dorsal cortecies at the level of cortical layer III 24 h following injection of either vehicle (**a**, **b**) or endothelin-1 (**c**, **d**). Position of injection sites are indicated. Both thionin (**a**, **c**) and TUNEL (**b**, **d**) staining results are shown. **e–h** Coronal sections through the dorsal cortex 200 µm distal to cannula infusion site. Arrowheads mark relative position of the injection site in the Z plane. Relative injury following injection of vehicle (**e**, **f**) or ET-1 (**g**, **h**) at 24 h is shown with dashed lines in (**e**) and (**g**) indicating principle zone of injury. Both thionin (**e**, **g**) and TUNEL (**f**, **h**) staining results are shown. White dashed lines in (**f**) and (**h**) denotes cortical limits. **i–k** Coronal view of TTC staining 24 h following cortical injection of endothelin-1 (white arrowheads). **i-j** Coronal tissue slices demonstrating contralateral and ipsilateral (white arrows) corticies. **k** Tissue cryosection denoting formazan reduced 1,3,5-triphenylformazan crystals (black arrows) in contralateral cortex and ipsilateral vascular collateral. Region proximal to endothelin-1 injection shows loss of TTC reduced product highlighted by the dashed circle. Scale bars are as indicated

proximal at 24 h post-injury. By contrast coronal sections taken 200 µm distal to the site of endothelin-1 infusion (Fig. 3a) revealed no such laminar distribution of activated caspase-3 positive cells. Examination of comparable zones within the contralateral cortex of treated animals revealed no activated caspase-3 positive cells (Fig. 3c, d). To examine the cellular morphology of ischemic cells in greater detail, cortical ultrastructure (layer V) was examined by electron microscopy. These studies demonstrate that in the absence of endothelin-1 relatively little cortical cell death is observed in this zone and neurons exhibit typical cellular architectures (Fig. 4a, b). By contrast animals receiving endothelin-1 exhibited significant levels of cortical cell death in this region which was frequently apoptotic in character (Fig. 4c–h, orange arrowheads). In addition, smaller numbers of cells also exhibited features of necrosis (Fig. 4e–h, red arrowheads).

In order to better define the nature and distribution of cell death occurring within the cortex in the presence of endothelin-1, horizontal cross sections were TUNEL labeled in conjunction with either neuronal (NeuN) or astroglial (GFAP) immunohistochemical markers (Fig. 5a, b). Together these markers identify approximately $94 \pm 3\%$ of the TUNEL positive cells observed 24 h following endothelin-1 infusion. As shown in the aggregate plot in Fig. 5c, TUNEL positive cells induced by endothelin-1 treatment exhibited a $> 90\%$ coincidence detection with NeuN. By contrast $< 5\%$ of GFAP positive astrocytes were positive for TUNEL. Thus the cell death observed following endothelin-1 treatment principally affects NeuN positive cortical neurons in the first 24 h.

Genetic loss of caspase-3 reduces levels of endothelin-1-mediated cortical neuronal injury

Given that findings from cell labeling and ultrastructure studies suggested that apoptosis plays a significant role in regulating endothelin-1-mediated death of cortical neurons, we examined the extent to which caspase-3 plays a direct role in regulating this death in vivo during the first 24 h period. As shown in Fig. 6a–d, caspase-3 null mice exhibit a reduction in their extent of cellular injury compared to caspase-3 wildtype and heterozygous littermates, particularly in zones more distal to the site of endothelin-1 injection. Observed reduction in levels of cellular injury as denoted by thionin staining (Fig. 6a, c) is mirrored by reductions in numbers of TUNEL positive cells at all layers of the cortex (Fig. 6b, d). With respect to lesion volume, caspase-3 null mice exhibited an approximately 60% reduction in total lesion volume compared to age matched wild-type controls and caspase-3 heterozygotes (Fig. 6e). To better understand mechanisms of the reduction in cellular injury seen in caspase-3 mice, we once again examined the cellular ultrastructure of layer V cortical neurons at sites 200 µm distal to the application of endothelin-1. Beyond reductions seen in total numbers of dying neurons (Figs. 6e,7a, b) we observed a lower percentage of dying neurons exhibiting features of apoptosis, and a higher percentage displayed necroptotic features (Fig. 7c–h) compared to that seen in endothelin-1 treated wild-type animals (WT: 54% apoptotic, 46% necroptotic versus 42% apoptotic, 58% necroptotic in caspase-3 null mice, $n = 80$). These changes agree well with the observed reduction in lesion volume if it arises as a result of rescue of the population of apoptotic neurons alone.

Loss of caspase-3 does not alter granulocyte infiltration, levels of microglial activation and caspase-7 activation

EM analysis of vascular arterioles proximal to cannula insertion 24 h following endothelin-1 treatment revealed the presence of locally infiltrating neutrophils in both wildtype and caspase-3 null mice (Fig. 8a, b). Further, horizontal sections were stained for CD11b to highlight populations of granulocytes, monocyte/macrophages and microglia. In all cases the majority ($> 80\%$) of CD11b positive cells were confined to regions proximal (< 200 µm from) to the position of cannula placement 24 h post-treatment. An example of the typical spatial distribution of CD11b cells is shown in Fig. 8c (cannula placement—black arrowhead; CD11b positive cells egressing from injured tissue vasculature—dark red arrowhead). Within comparative zones of contralateral (untreated) cortices, only low levels of microglial staining are observed (Fig. 8d). Higher resolution examples demonstrating the pattern of CD11b staining are shown in Fig. 8e, f respectively for wildtype and

caspase-3 knockout mice (black arrowheads—edge of cannula placement). Analysis of the total number of CD11b positive cells within zones 0–200, 200–300 and 300–400 µm of cannula placement (circular ROI) revealed no significant differences between wildtype and caspase-3 null groups, indicating that loss of caspase-3 does not alter the degree of activation or infiltration of CD11b positive cells within the first 24 h of treatment (data not shown).

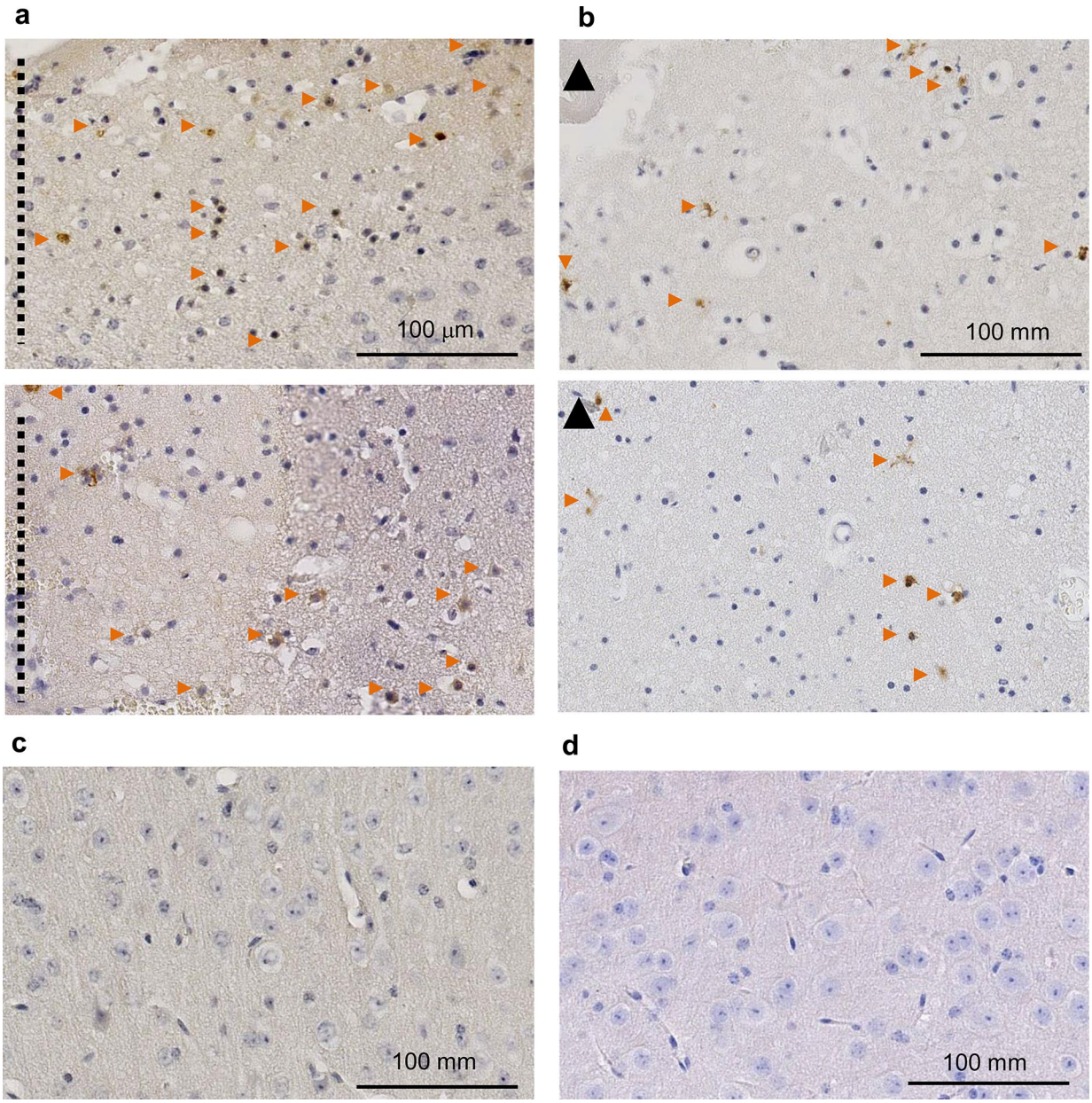

Fig. 3 Endothelin-1 induced caspase-3 activation in the cortex 24 h following infusion. **a**, **b** Examples are shown of the pattern of caspase-3 activation observed in the cortex in both the coronal (**a**, xy axis) or horizontal (**b**, layer III) plane. Dotted line and black arrowheads indicate relative position of cannula placement (coronal: XY, horizontal: Z axes respectively). **c**, **d** Examples of activated caspase-3 staining pattern in contralateral cortex in comparative coronal (**c**) and horizontal (**d**) planes. For each panel peroxidase stained activated caspase-3 positive cells are indicated by brown arrowheads. Scale bars are as indicated

Fig. 4 Electron microscopy of cortical neuron morphology. Shown ▶ are typical layer V neuron morphology 24 h following infusion of vehicle (**a**, **b**) or endothelin-1 (**c–h**) into the cortex. Few dying neurons are observed in vehicle infused corticies beyond the region of mechanical injury (**a**, **b** blue arrowhead demonstrates healthy neurons). **c–h** By contrast ET-1 treated mice demonstrate diffuse array of neurons with apoptotic morphology (yellow arrowheads) as well as lower numbers of cells with necrotic/necroptotic morphology (red arrowheads). For each figure scale bars are as indicated (Color figure online)

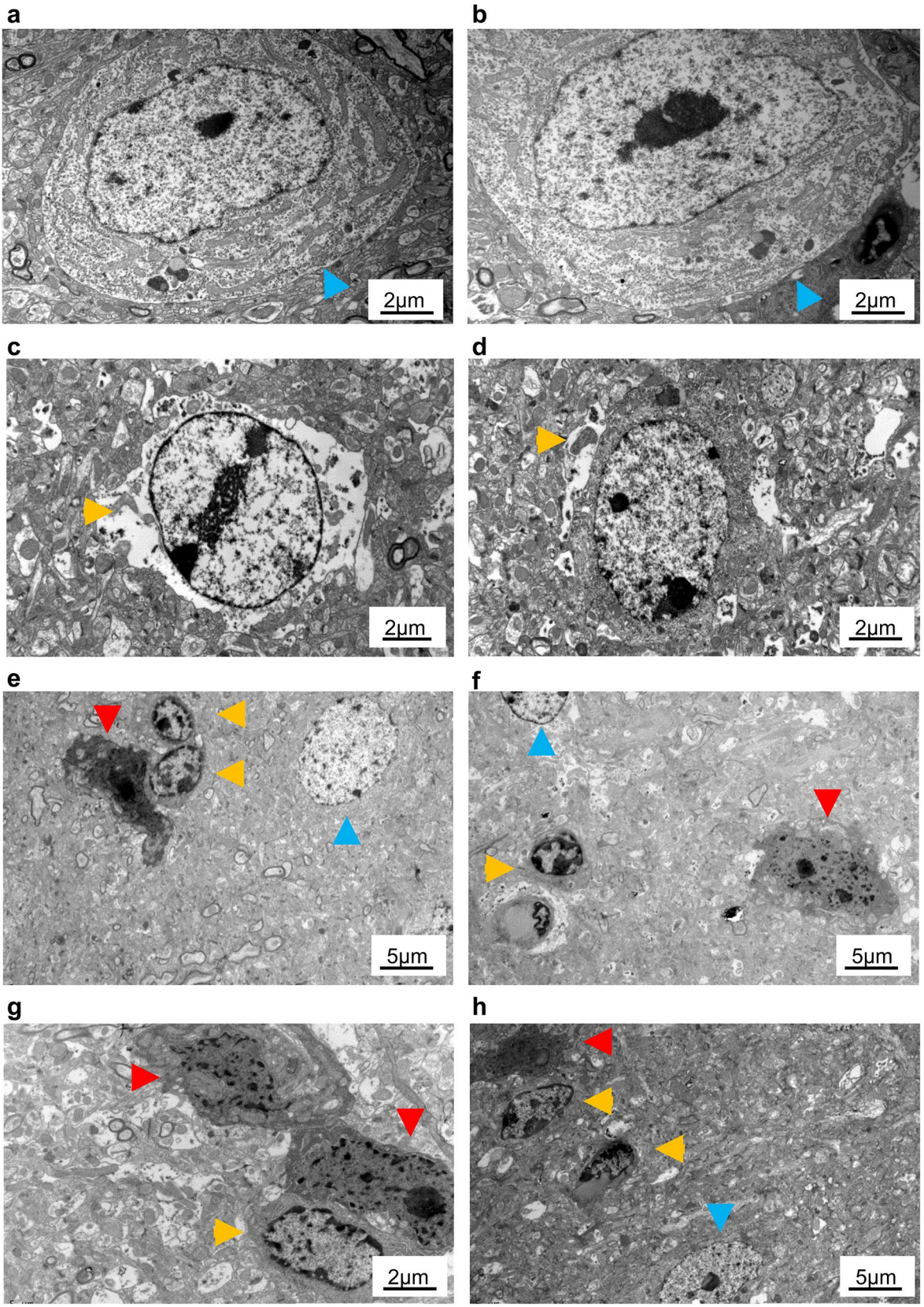
a
2μm
b
2μm
c
2μm
d
2μm
e
5μm
f
5μm
g
2μm
h
5μm

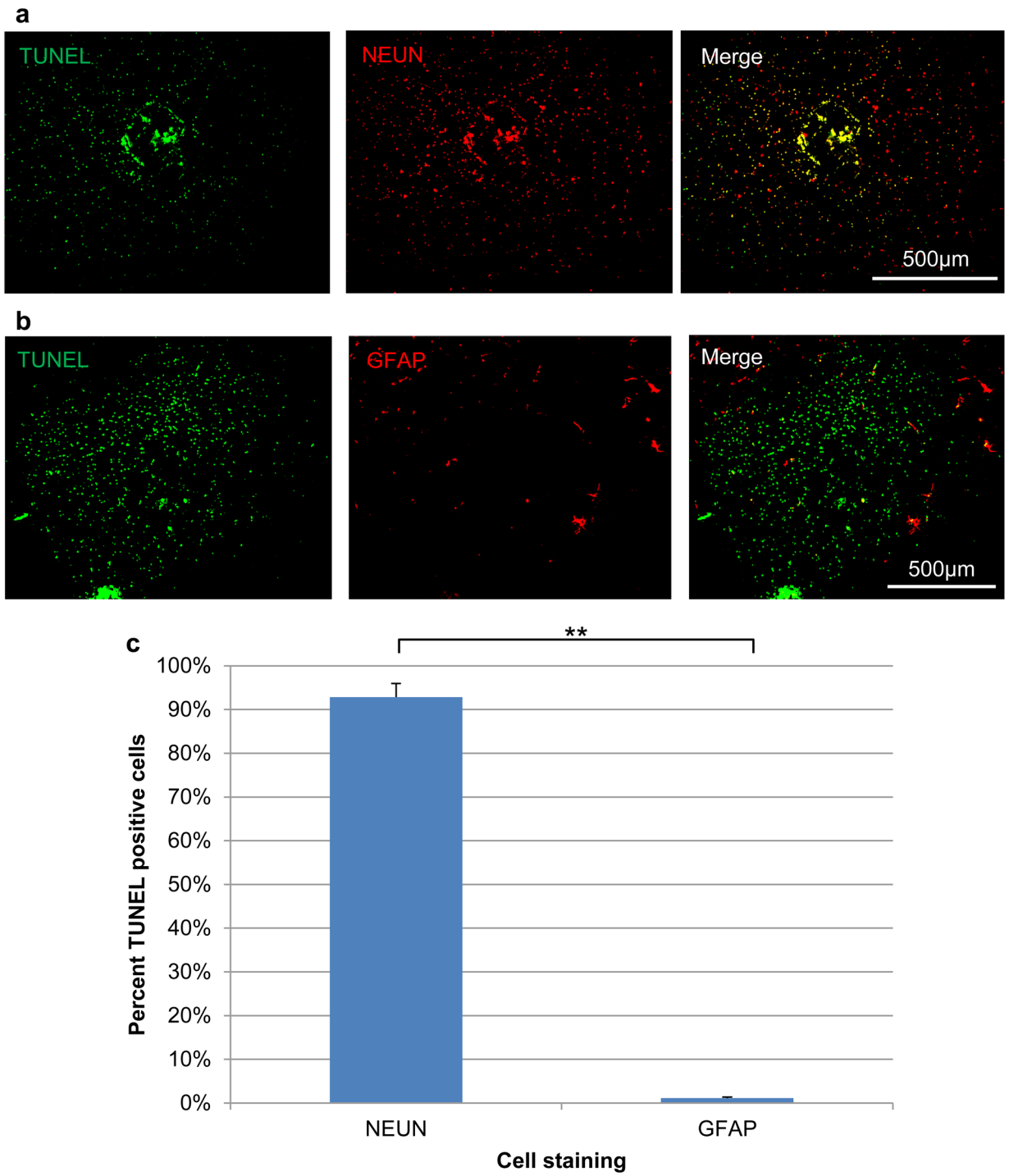

Fig. 5 Analysis of affected cell type following endothelin-1 infusion. Pattern of TUNEL positive (green) cellular profiles observed relative to neuronal marker NeuN (**a**) or GFAP (**b**) in horizontal plane 24 h following endothelin-1 treatment. Merge of TUNEL and marker is indicated on the right. Scale as indicated. **c** Distributon plot of TUNEL positive cells as a percent of cellular markers examined ± S.E.M. (n = 3 sections/animal, 4 animals per set). **Indicates statistical significance at $p < 0.01$ (Color figure online)

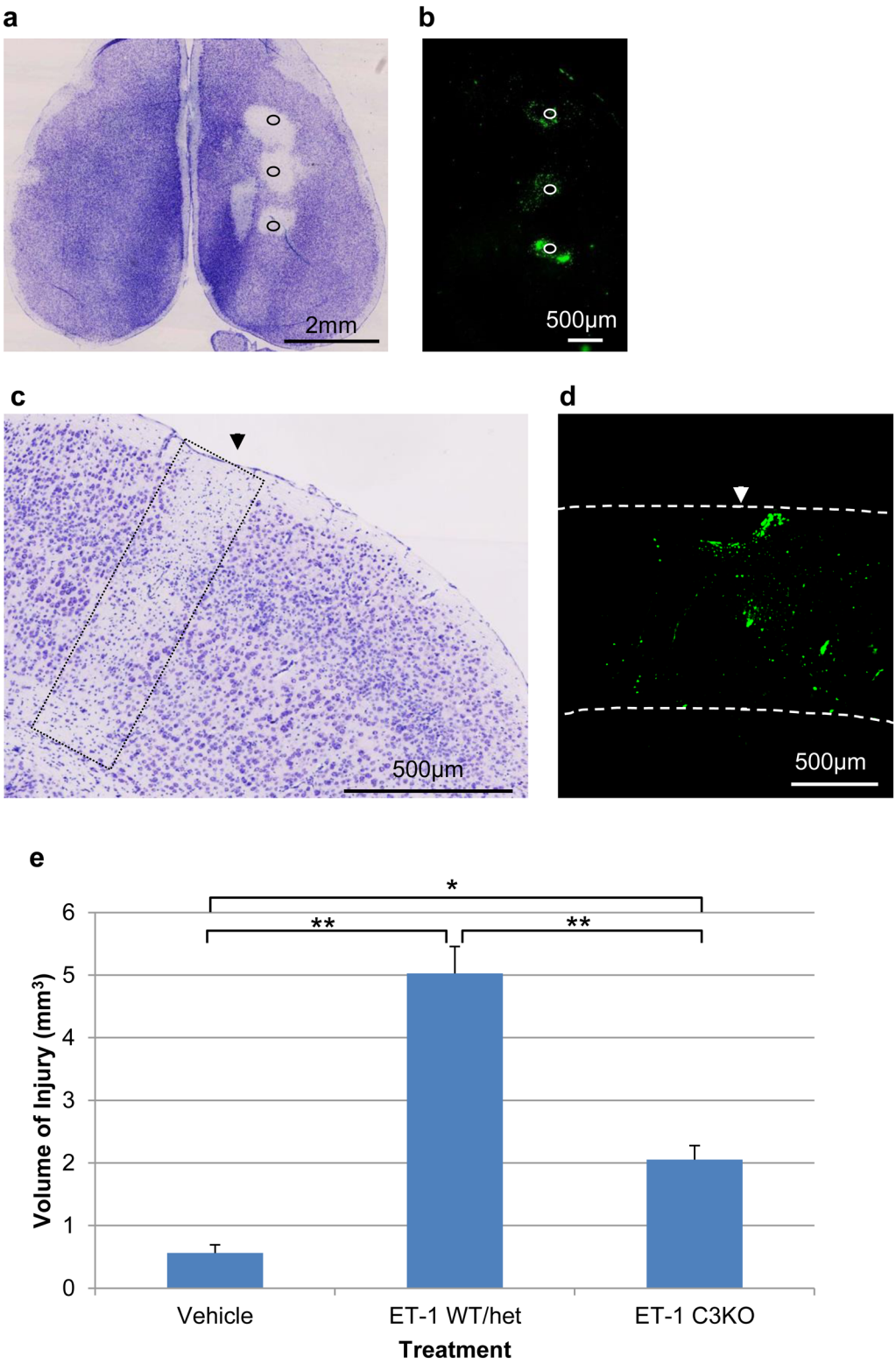

Fig. 6 Loss of Caspase-3 reduces levels of endothelin-1-induced ischemic injury. As demonstrated by thionin (**a**, **c**) and TUNEL (**b**, **d**) staining in horizontal (**a**, **b**) and coronal (**c**, **d**) planes. Caspase-3 null mice exhibit a reduction in total cellular loss 24 h following endothelin-1 treatment. Relative position of injection sites are indicated by circle (**a**, **b**) and arrowheads (**c**, **d**). Black dashed lines in (**c**) denotes the primary region of injury. White dashed lines in (**d**) denotes limits of cortex. **e** Analysis of total volume of cortical injury in vehicle, ET-1 treated wild-type/heterozygotes controls, and caspase-3 null mice ± S.E.M. (n = 5, 7 and 6 respectively). * Represents statistically significant difference with respect to volume of injury at $p < 0.05$ and ** represents statistical significance at $p < 0.01$

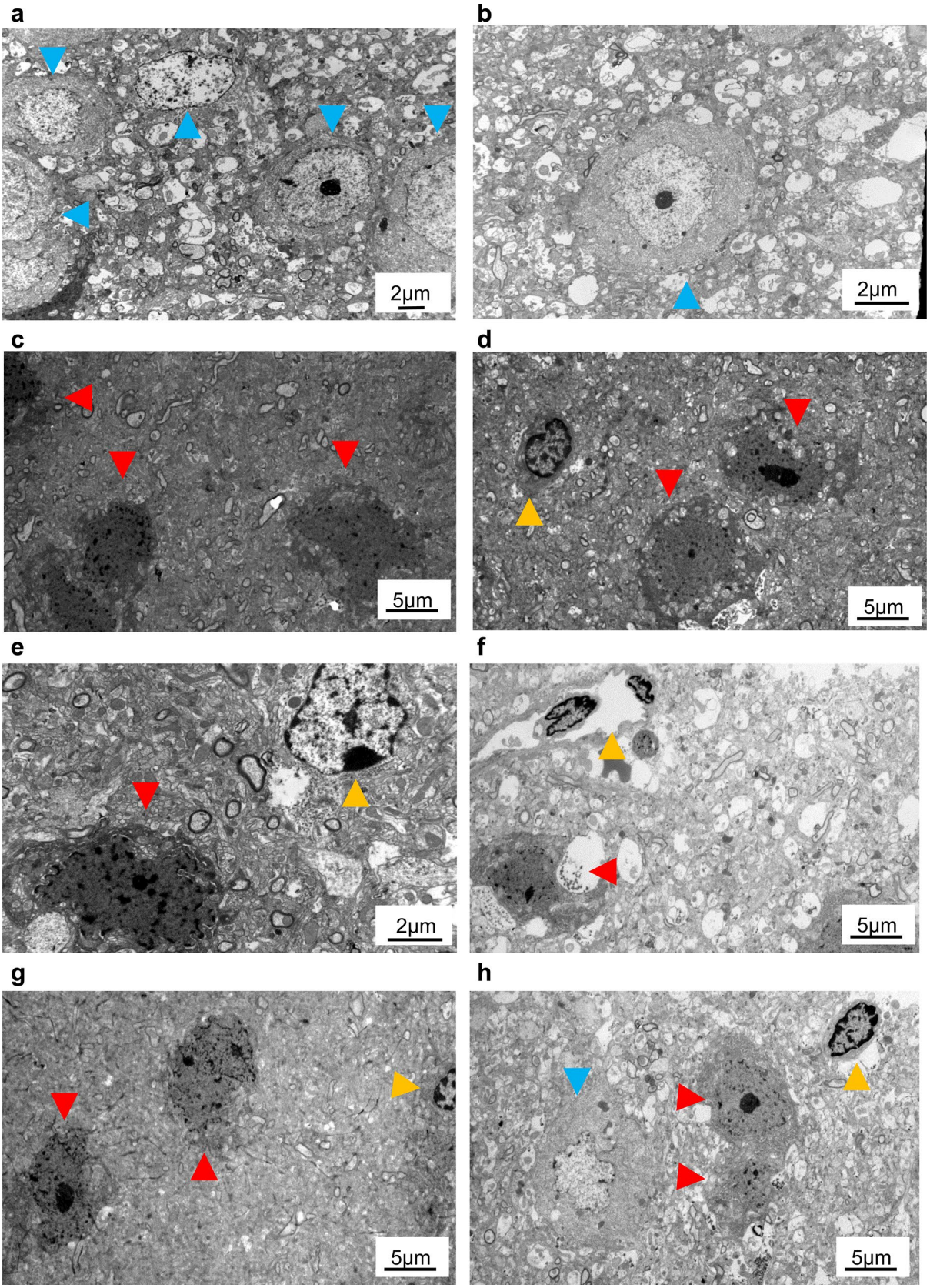
a
2μm
b
2μm
c
5μm
d
5μm
e
2μm
f
5μm
g
5μm
h
5μm

◂**Fig. 7** Electron microscopy of cellular ultrastructure in caspase-3 null mice. **a**, **b** Typical layer V morphology of healthy neurons in caspase-3 null mice 24 h following infusion of ET-1. Blue arrowhead highlight increased observation of healthy cells following ET-1 treatment in mutants compared to wild-type/heterozygote controls. **c–h** Examples of layer V dying neuron morphology 24 h following endothelin-1 treatment. Dying cortical neurons in caspase-3 null mice exhibit a relative enhancement in their number of necrotic/necroptotic (red arrowheads) versus apoptotic (yellow arrowheads) neurons. Scale bars are as indicated (Color figure online)

In order to further discriminate and characterize the pattern of local cellular activity induced by endothelin-1 treatment, staining the well-characterized macrophage/microglial marker F4/80 was examined. F4/80 was utilized as it excludes granulocyte populations and in our hands appears more sensitive than CD11b for the detection of tissue resident phagocytic cells in murine brain. As shown in Fig. 9a, b respectively, a disseminated network of F4/80 positive cells are observed in both wildtype and caspase-3 null endothelin-1 treated tissues within a zone of 350 μm from cannula placement by 24 h post-treatment.

Though loss of caspase-3 results in a substantial reduction in endothelin-1-mediated cell death; the resulting injury observed in these animals is still significantly greater than that seen in vehicle controls alone (Fig. 6e). While this cell death may be due to alternative (i.e. necroptosis or other) cell death mechanisms, we notably continued to observe a degree of apoptotic cell death (Fig. 7d–h) in endothelin-1 treated caspase-3 null mice. In order to better understand the nature of this phenomenon we examined hypoxic cortical zones for their pattern of activated caspase-7. As observed in both wildtype and caspase-3 null mice respectively (Fig. 9c, d) 24 h following endothelin-1 treatment, neurons expressing activated caspase-7 (orange arrowheads) are interspersed within these zones with neurons which do not express this activated caspase-7 (blue arrowheads). Thus within the ischemic cortex there exist neural subpopulations which exhibit distinct programs of executioner caspase activation.

Discussion

A wide array of pharmacologic agents have been examined in animal models of ischemic injury. Yet despite reports of efficacy for a number of such trials, these agents frequently fail to reproduce similar findings in clinical trials [16–18]. The lack of identification of other therapeutic agents (beyond thrombolytics) capable of the acute neuroprotection of ischemic tissues over the past two decades has caused some to question the underlying animal models or procedures utilized. Yet equivalency observed between rodents and humans in their pattern of cell death and the efficacy of thrombolytic therapies following ischemic injury suggest that the underlying molecular mechanisms governing such injuries is conserved [41]. As such issues of the inherent variability within given models and the nature and extent of the neurologic injuries induced have become targets of investigation. Irreducible variabilities in wide-area ischemic models dependent upon stochastic vasculature innervation with substantial sub-cortical injury such as MCAO have highlighted the need for localized ischemic models of low variability which can be used to target specific cortical regions which more closely resemble the most common ischemic cortical injuries seen in humans.

Despite prior studies demonstrating that stereotactic application of endothelin-1 can be utilized to induce cortical lesions in rats [29–31], controversy exists as to whether this approach can reliably induce ischemic injury in mice [28, 32–34, 42]. In the present study we demonstrate that intracortical injection of 160 pmol of endothelin-1 in the absence of other agents or genetic modifications results in a highly reproducible pattern of ischemic cell death in both CD1 and C57BL/6J mice as shown by trypan blue, thionin and TTC staining. As demonstrated in vivo, the large azo dye trypan blue is prevented from extravasation in healthy vascular tissues due to the presence of an intact endothelium [43, 44]. However as expected 24 h following endothelin-1 treatment trypan blue extravasation is markedly enhanced in zones of treatment. As described previously [45–47], sustained hypoxia induces breakdown of a number of cellular constituents including ribosomal RNA and the rough endoplasmic reticulum (Nissl substance). In neurons this is change readily detected by metachromatic dyes such as thionin. This method can thus be used to assess cytological features of neural cells in an unbiased manner in minutes (as opposed to immunohistochemical methods), and whose interpretation is not typically altered as a result of changes to a single or small groups of proteins. With respect to hypoxic changes, loss of thionin metachromasia manifest as a result of degeneration of DNA, RNA (to which thionin binds electrostatically) and resulting loss of Nissl substance in the rough endoplasmic reticulum [45–48]. In these circumstances hypoxic injury can clearly be delineated in thionin stained sections as zones markedly lower intensity (ghost staining) and the presence of compacted argyrophilic ‘dark’ neurons [45–47, 49, 50]. Such analysis demonstrates that the extent of injury is significantly expanded in the presence of endothelin-1 compared to vehicle controls. Similarly TTC staining demarcates regions of viable versus hypoxic tissue through reduction of the initially colourless triphenyl tetrazolium chloride to a red formazan product via mitochondrial dehydrogenase activity [51], and is therefore often utilized to identify levels of cellular respiration in tissue [51, 52]. Consistent with observations from

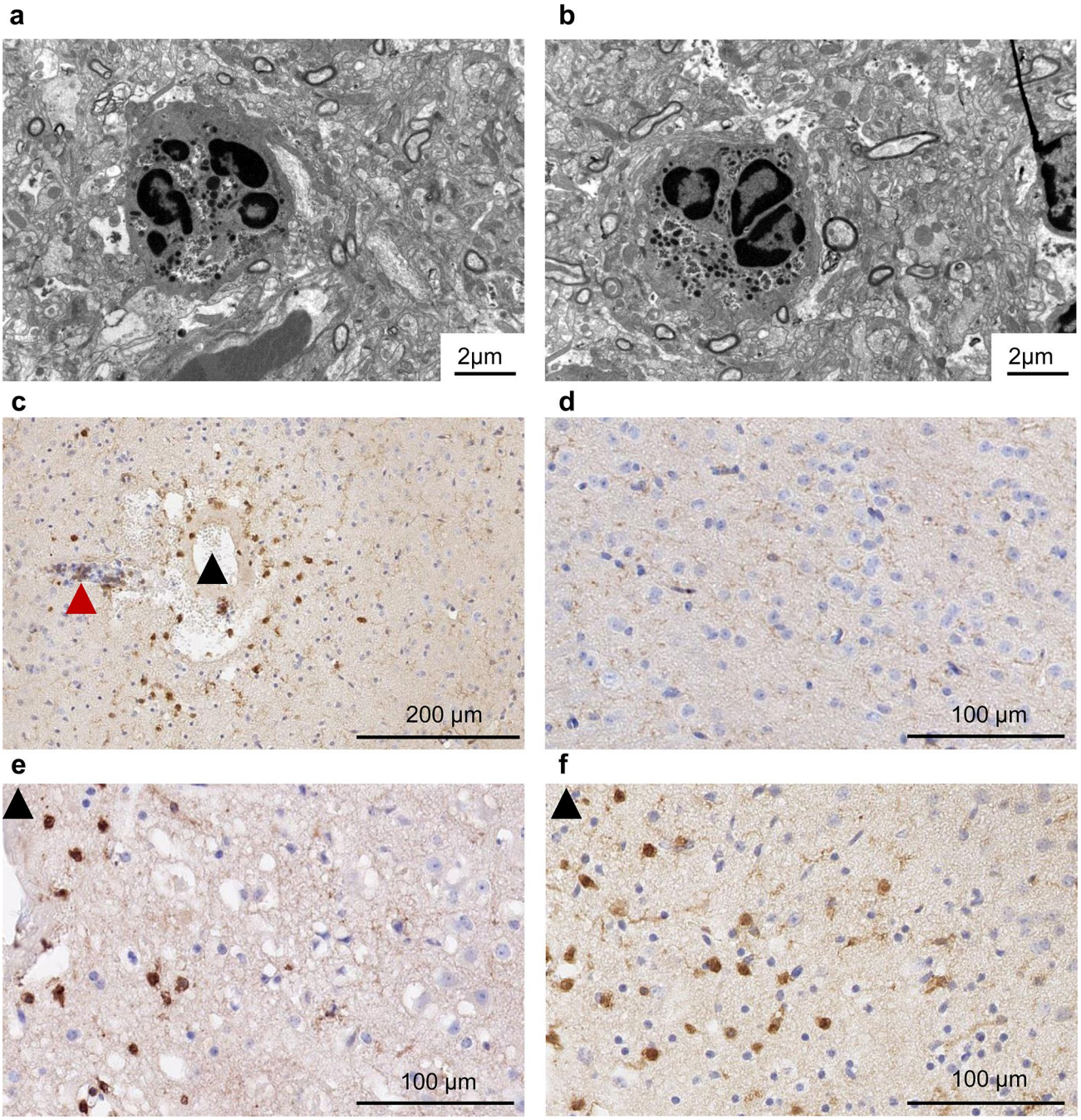

Fig. 8 Granulocyte infiltration in the cortex following endothelin-1 treatment. As shown by EM, neutrophils are observed within layer V brain parenchyma 24 h following endothelin-1 treatment as seen in both wildtype (**a**) and caspase-3 null (**b**) mice. **c–f** Distribution of CD11b-positive cells in the brain. Horizontal sections are shown. Black arrowheads indicate relative position of endothelin-1 infusion. Dark red arrowhead highlights CD11b positive cells egressing from injured tissue vasculature. **c** Spatial distribution of CD11b positive cells relative to endothelin-1 infusion. **d** Pattern of CD11b staining observed in comparable region and layer of contralateral hemisphere (no endothelin-1 treatment). **e–f** Examples of distribution of CD11b-positive cells in wildtype (**e**) and caspase-3 null (**f**) mice. Scale bars as indicated (Color figure online)

thionin staining and trypan blue infusion, TTC treatment demonstrates that endothelin-1 enhances cortical tissue hypoxia compared to controls.

Analysis of cell type specificity and EM profile analysis indicates that the endothelin-1 mediated cell death which occurs during the first 24 h principally affects neurons. This injury is confined to the cortex and shows substantially low

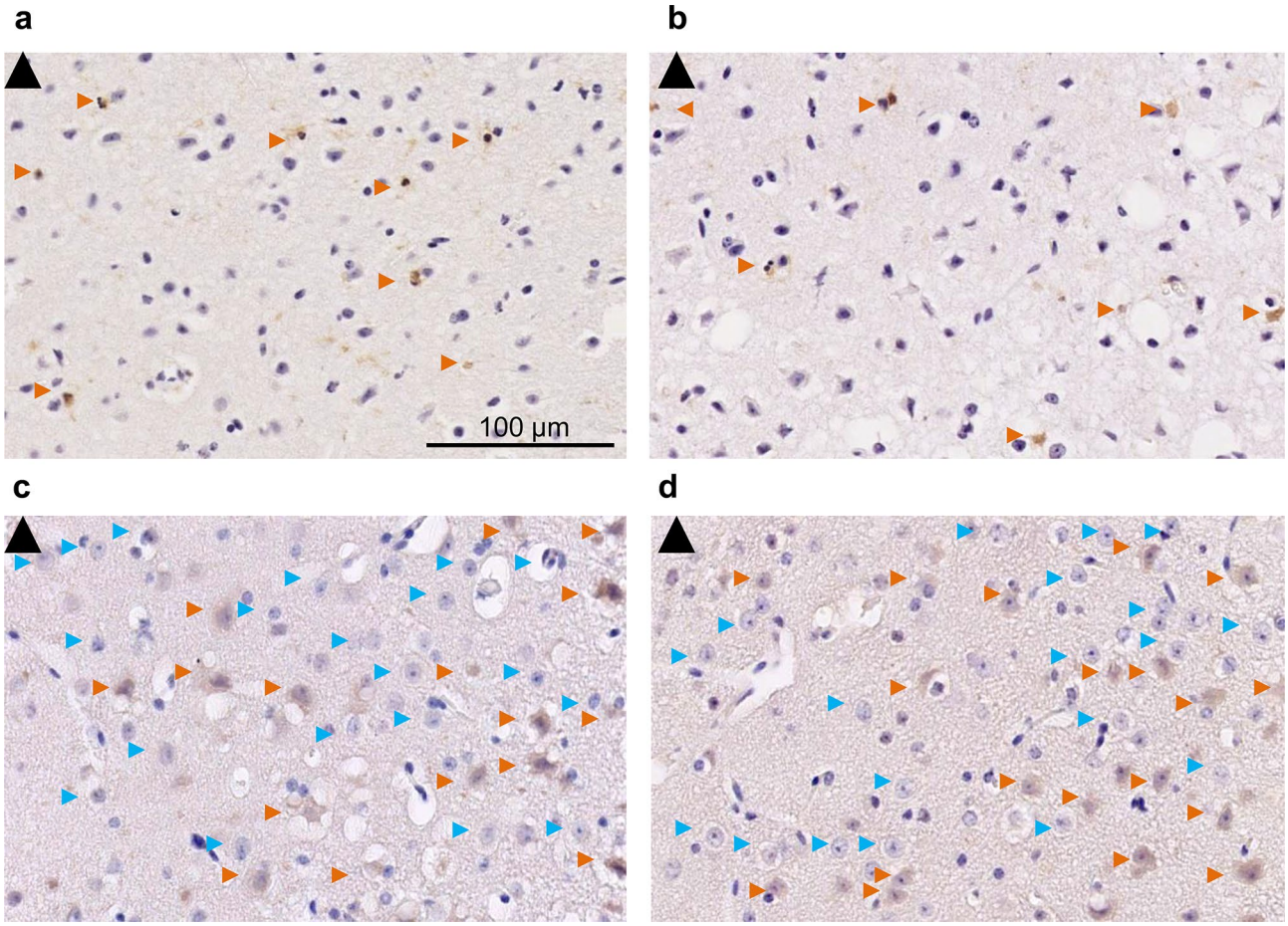

Fig. 9 Distribution of F4/80 and caspase-7 activation in wildtype and caspase-3 null mice. **a**, **b** Distribution of F4/80-positive cells in wildtype (**a**) and caspase-3 null (**b**) mice. Horizontal sections are shown. Black arrowheads indicate relative position of endothelin-1 infusion. **c**, **d** Distribution of activated caspase-7 in wildtype (**c**) and caspase-3 null (**d**) mice. For each panel peroxidase stained F4/80 or activated caspase-7 positive cells are indicated by brown arrowheads. Blue arrowheads in (**c**) and (**d**) denotes activated caspase-7 negative cells. Scale for all photomicrographs are as indicated in (**a**) (Color figure online)

sample-to-sample variability compared to models such as MCAO due to the geometry of the injury [24]. Application of endothelin-1 has previously been used to induce cortical lesions in FVB/N mice; the histologic and behavioral effects of which have been documented 14 days following injury [33]. However numerous studies in rodent, primates and man have highlighted the critical importance of early signaling events regulating levels of induction with respect to neuronal cell death [53–58]. Therefore understanding and mitigating these events is critical in maintaining 'at risk' ischemic tissues. As an initial step in this process we have sought to better characterize several aspects of the cellular and molecular nature of such early ischemic events. Because of previous mixed results reported in mice with respect to endothelin-1 efficacy, we sought to first minimize fluidic volumes, below that seen in prior studies (160 pmol in 400 nL) in order to reduce confounding variables such as mechanical and/or pressure-induced injury arising from infusion. The cortical results we obtained compare favorably to those described by Soylu et al. [28] who utilized a somewhat larger bolus volume (400 pmol in 1000 nL) to effect intracortical injury in CD1 mice or mice expressing human the equilibrative nucleoside transporter 1 (hENT1), demonstrating reduced local cerebral blood flow to $12.5 \pm 2.0\%$ 4 h post-injection returning to $45.2 \pm 6.3\%$ in CD1's by 48 h as determined by magnetic resonance imaging. Infarct sizes observed for CD1 mice in this study compare favorably with what we observed in adult CD1 and inbred C57BL/6J mice: [Saline: 0.3 ± 0.1 mm^3 for CD1 versus 0.53 ± 0.2 mm^3 in C57BL/6J; ET-1: 5.4 ± 0.8 mm^3 for CD1 versus 5.0 ± 0.5 mm^3 for C56Bl/6J]. In contrast the results described by Wang et al. [42] in C57BL/6J mice utilizing injections volumes of up to 1000 nL of 1 mg/mL endothelin-1 reported minimal cortical lesions upon analysis at 6 days post-injection. In order to distinguish later compensatory changes which may occur at lesion sites following injury from immediate early events,

we have chosen to analyze lesions 24 h following endothelin-1 treatment. With respect to differences between the above and other endothelin-1 studies in mice it should also be noted that we have observed significant batch-to-batch variability in endothelin-1 supplied from several vendors and thus recommend direct biologic testing of batches prior to undertaking assays.

Results of unbiased cellular (EM) and molecular analyses (thionin versus TUNEL labeling, activated caspase-3 versus activated caspase-7 staining), suggest that apoptosis is the most common form of cell death induced within ischemic tissues. Consistent with this the majority of cells identified within the injured region using thionin staining are TUNEL positive. While TUNEL staining is widely utilized as a marker of apoptosis, it is possible that in some circumstances TUNEL positive cells could arise through conditions other than classical apoptotic cell death. Thus in order to better delineate between apoptotic and necrotic cell death in the present study, several additional cellular and molecular markers have been utilized. These include markers denoting activation of the apoptotic executioners caspase 3 and 7 as well as changes to cell ultrastructure as detailed by electron microscopy; widely considered to be a gold standard with respect to identification of cell death isoform. Consistent with the stated TUNEL findings, examination of the pattern of activated caspase-3 staining within hypoxic regions demonstrated the presence of a large number of activated caspase-3-positive neurons throughout the zone of injury with a preponderance of such cells 200–300 μm distal to the primary lesion site 24 h following endothelin-1 treatment. Similarly, EM analysis of the cellular morphology of cortical cell death in the zone of injury primarily exhibited apoptotic features, with fewer cells exhibiting necrotic features. In order to determine the causal role which apoptotic executioner caspases play in regulating the observed neuronal death, we examined the effects of genetic deletion of caspase-3 on cell loss in this paradigm. Loss of caspase-3 resulted in a ~ 60% reduction in overall lesion volume as shown by thionin staining and substantial reduction in numbers of TUNEL-positive cells within the ischemic zone of injury following endothelin-1 application (Fig. 6). Despite this, examination of ischemic regions in caspase-3 null mice by electron microscopy revealed the continued presence of a population of dying neurons exhibiting apoptotic morphology. Examination of these ischemic tissues for their pattern of activated caspase-7 revealed a network of both caspase-7 positive and negative neurons throughout these regions 24 h following the application of endothelin-1. The comparable activation mechanics and similar though not identical cellular target profiles of these cysteine proteases [59–61] may allow caspase-7 to compensate for loss of caspase-3 in those neurons that express it at sufficient concentrations. However such compensation cannot completely mirror the functional roles of caspase-3 as demonstrated by the pattern of activated caspase-7 staining seen within cortical neurons and the reduction in hypoxic injury observed in caspase-3 null mice; indicating the presence of cortical subpopulations with different compositions of executioner caspases. Indeed the existence of such subpopulations is further highlighted by the presence of neurons that die by an alternative pathway (necroptotic/necrotic) were not affected by loss of caspase-3 as determined by electron microscopy.

In the present study we have focused on the early cellular properties induced by endothelin-1 treatment within the cortex as this has not been examined in detail in this model previously. In addition to the direct action of endothelin-1 and caspase activation on cortical neurons, potential cellular effects may also arise as a secondary consequence of infiltrating and/or resident phagocytic cells. To gain insight into the temporal aspect of such effects, we focused on the critical 24 h period following injury. Given that loss of caspase-3 resulted in a substantial reduction in lesion volume and cell death at this time, we examined whether the complete absence of caspase-3 activity altered secondary responses such as infiltration of granulocytes or the activity of resident microglia. Such investigation is based on the idea that loss of caspase-3 expression might alter cell death signaling in such a way as to modify danger signals arising from degenerating neurons. As observed in wild-type mice, endothelin-1 infusion resulted in the accumulation of neutrophils proximal to the infusion site by 24 h post-treatment as seen by electron microscopy and CD11b staining. Notably no significant difference was observed in the pattern or degree of accumulation of these cells in caspase-3 null mice compared to wild-types. As CD11b (Ly-40, *Itgam*) identifies granulocytes, monocyte/macrophages and microglia in the mammalian CNS [62–66], we further examined endothelin-1 treated cortices with the macrophage/microglial marker F4/80 [63–65] to more clearly distinguish this cellular population. Comparative analysis of CD11b versus F4/80 immunohistochemistry demonstrates that the majority of CD11b staining is observed proximal to the infusion site arising from infiltrating granulocytes (neutrophils). By contrast F4/80 positive microglia exhibits only a diffuse scattered network staining 24 h post endothelin-1 treatment. Similar to CD11b, no significant difference in the pattern or extent of F4/80 (Ly-71, *Emr1*) staining is seen between wildtype and caspase-3 null mice, suggesting that the effects observed in the absence of caspase-3 arise principally due to direct inhibition of PCD signaling within caspase-3 sensitive cortical subpopulations. Such effects thus regulate a critical early component of the response of neurons to endothelin-1-induced hypoxia/reperfusion injury, with granulocyte and

microglial mediated effects likely rising in prominence during later phases of injury response.

Acknowledgements We would like to thank Kyle Gill and Ryan Harrietha for genotyping assistance; Zoe Winterton-Perks for assistance with histology; Zhihua Huang and Lida Du for assistance with TTC staining; and Ali Darbandi and Doug Holmyard for electron microscopy assistance.

Funding This study has been funded by grants awarded to J.H. from Natural Sciences and Engineering Research Council of Canada (NSERC) (RGPIN 298553-12) and Heart and Stroke Society of Canada (72043506). C.D.S. additionally received scholarship funding from Natural Sciences and Engineering Research Council of Canada (NSERC) and Queen Elizabeth II Graduate Scholarships in Science & Technology- Merck Company of Canada.

Compliance with ethical standards

Conflict of interest The authors declare no conflicts of interest.

Ethical approval The experiments performed in this study comply with ethical requirements and laws as discussed above.

References

1. World Health Organization (2004) Global burden of stroke. http://www.who.int/cardiovascular_diseases/en/cvd_atlas_15_burden_stroke.pdf. Accessed 4 May 4 2016
2. Simonetti G, Stefanini M, Konda D, Marziali S, Da Ros V, Chiaravalloti A, Pampana E, Gandini R (2013) Endovascular management of acute stroke. J Cardiovasc Surg 54(1):101–114
3. Albers GW, Goyal M, Jahan R, Bonafe A, Diener HC, Levy EI, Pereira VM, Cognard C, Cohen DJ, Hacke W, Jansen O, Jovin TG, Mattle HP, Nogueira RG, Siddiqui AH, Yavagal DR, Baxter BW, Devlin TG, Lopes DK, Reddy VK, de Rochemont RduM, Singer OC, Bammer R, Saver JL (2016) Ischemic core and hypoperfusion volumes predict infarct size in SWIFT PRIME. Ann Neurol 79(1):76–89
4. Yuan J (2009) Neuroprotective strategies targeting apoptotic and necrotic cell death for stroke. Apoptosis 14(4):469–477
5. Fulda S, Debatin KM (2006) Extrinsic versus intrinsic apoptosis pathways in anticancer chemotherapy. Oncogene 25(34):4798–4811
6. Adams JM (2003) Ways of dying: multiple pathways to apoptosis. Genes Dev 17(20):2481–2495
7. Alberts B, Johnson A, Lewis J, Raff M, Roberts K, Walter P (2008) Molecular biology of the cell, 5th edn. Garland Science, Taylor and Francis Group, New York
8. Cain K, Bratton SB, Cohen GM (2002) The Apaf-1 apoptosome: a large caspase-activating complex. Biochimie 84(2–3):203–214
9. Cullen SP, Martin SJ (2009) Caspase activation pathways: some recent progress. Cell Death Differ 16(7):935–938
10. Yuan S, Akey CW (2013) Apoptosome structure, assembly, and procaspase activation. Structure 21(4):501–515
11. Donepudi M, Grutter MG (2002) Structure and zymogen activation of caspases. Biophys Chem 101–102:145–153
12. Sakahira H, Enari M, Nagata S (1998) Cleavage of CAD inhibitor in CAD activation and DNA degradation during apoptosis. Nature 391(6662):96–99
13. Kurokawa M, Kornbluth S (2009) Caspases and kinases in a death grip. Cell 138(5):838–854
14. Chay KO, Park SS, Mushinski JF (2002) Linkage of caspase-mediated degradation of paxillin to apoptosis in Ba/F3 murine pro-B lymphocytes. J Biol Chem 277(17):14521–14529
15. Del Zoppo GJ, Saver JL, Jauch EC, Adams HP Jr (2009) Expansion of the time window for treatment of acute ischemic stroke with intravenous tissue plasminogen activator: a science advisory from the American Heart Association/American Stroke Association. Stroke 40(8):2945–2948
16. Ford GA (2008) Clinical pharmacological issues in the development of acute stroke therapies. Br J Pharmacol 153(Suppl 1):S112–S119
17. Ginsberg MD (2009) Current status of neuroprotection for cerebral ischemia: synoptic overview. Stroke 40(3 Suppl):S111–S114
18. Cheng YD, Al-Khoury L, Zivin JA (2004) Neuroprotection for ischemic stroke: two decades of success and failure. NeuroRx 1(1):36–45
19. Mestas J, Hughes CCW (2004) Of mice and not men: differences between mouse and human immunology. J Immunol 172(5):2731
20. Carmichael ST (2005) Rodent models of focal stroke: size, mechanism, and purpose. NeuroRx 2(3):396–409
21. Bacigaluppi M, Comi G, Hermann DM (2010) Animal models of ischemic stroke. Part two: modeling cerebral ischemia. Open Neurol J 4:34–38
22. Dulli D, D'Alessio DJ, Palta M, Levine RL, Schutta HS (1998) Differentiation of acute cortical and subcortical ischemic stroke by risk factors and clinical examination findings. Neuroepidemiology 17(2):80–89
23. Pulli B, Schaefer PW, Hakimelahi R, Chaudhry ZA, Lev MH, Hirsch JA, Gonzalez RG, Yoo AJ (2012) Acute ischemic stroke: infarct core estimation on CT angiography source images depends on CT angiography protocol. Radiology 262(2):593–604
24. Ghanavati S, Lerch JP, Sled JG (2014) Automatic anatomical labeling of the complete cerebral vasculature in mouse models. Neuroimage 95:117–128
25. Macrae IM (2011) Preclinical stroke research–advantages and disadvantages of the most common rodent models of focal ischaemia. Br J Pharmacol 164(4):1062–1078
26. Sapira V, Cojocaru IM, Lilios G, Grigorian M, Cojocaru M (2010) Study of endothelin-1 in acute ischemic stroke. Rom J Intern Med 48(4):329–332
27. Macrae IM, Robinson MJ, Graham DI, Reid JL, McCulloch J (1993) Endothelin-1-induced reductions in cerebral blood flow: dose dependency, time course, and neuropathological consequences. J Cereb Blood Flow Metab 13(2):276–284
28. Soylu H, Zhang D, Buist R, Martin M, Albensi BC, Parkinson FE (2012) Intracortical injection of endothelin-1 induces cortical infarcts in mice: effect of neuronal expression of an adenosine transporter. Exp Transl Stroke Med 4(1):4
29. Fuxe K, Kurosawa N, Cintra A, Hallstrom A, Goiny M, Rosen L, Agnati LF, Ungerstedt U (1992) Involvement of local ischemia in endothelin-1 induced lesions of the neostriatum of the anaesthetized rat. Exp Brain Res 88(1):131–139
30. Windle V, Szymanska A, Granter-Button S, White C, Buist R, Peeling J, Corbett D (2006) An analysis of four different methods of producing focal cerebral ischemia with endothelin-1 in the rat. Exp Neurol 201(2):324–334
31. Gilmour G, Iversen SD, O'Neill MF, Bannerman DM (2004) The effects of intracortical endothelin-1 injections on skilled forelimb use: implications for modelling recovery of function after stroke. Behav Brain Res 150(1–2):171–183
32. Horie N, Maag AL, Hamilton SA, Shichinohe H, Bliss TM, Steinberg GK (2008) Mouse model of focal cerebral ischemia using endothelin-1. J Neurosci Methods 173(2):286–290

33. Roome RB, Bartlett RF, Jeffers M, Xiong J, Corbett D, Vanderluit JL (2014) A reproducible Endothelin-1 model of forelimb motor cortex stroke in the mouse. J Neurosci Methods 233:34–44
34. Tennant KA, Jones TA (2009) Sensorimotor behavioral effects of endothelin-1 induced small cortical infarcts in C57BL/6 mice. J Neurosci Methods 181(1):18–26
35. Woo M, Hakem R, Soengas MS, Duncan GS, Shahinian A, Kagi D, Hakem A, McCurrach M, Khoo W, Kaufman SA, Senaldi G, Howard T, Lowe SW, Mak TW (1998) Essential contribution of caspase 3/CPP32 to apoptosis and its associated nuclear changes. Genes Dev 12(6):806–819
36. Chan E, Kovacevic N, Ho SK, Henkelman RM, Henderson JT (2007) Development of a high resolution three-dimensional surgical atlas of the murine head for strains 129S1/SvImJ and C57Bl/6 J using magnetic resonance imaging and micro-computed tomography. Neuroscience 144(2):604–615
37. Xiong B, Li A, Lou Y, Chen S, Long B, Peng J, Yang Z, Xu T, Yang X, Li X, Jiang T, Luo Q, Gong H (2017) Precise cerebral vascular atlas in stereotaxic coordinates of whole mouse brain. Front Neuroanat 11:128
38. Sun HS, Xu B, Chen W, Xiao A, Turlova E, Alibraham A, Barszczyk A, Bae CY, Quan Y, Liu B, Pei L, Sun CL, Deurloo M, Feng ZP (2015) Neuronal K(ATP) channels mediate hypoxic preconditioning and reduce subsequent neonatal hypoxic-ischemic brain injury. Exp Neurol 263:161–171
39. Alibrahim A, Zhao LY, Bae CY, Barszczyk A, Sun CL, Wang GL, Sun HS (2013) Neuroprotective effects of volume-regulated anion channel blocker DCPIB on neonatal hypoxic-ischemic injury. Acta Pharmacol Sin 34(1):113–118
40. Sakai R, Henderson JT, O'Bryan JP, Elia AJ, Saxton TM, Pawson T (2000) The mammalian ShcB and ShcC phosphotyrosine docking proteins function in the maturation of sensory and sympathetic neurons. Neuron 28(3):819–833
41. Back T, Otto D, Kittner D, Schuler OG, Hennerici MG, Mennel HD (2007) Failure to improve the effect of thrombolysis by memantine in a rat embolic stroke model. Neurol Res 29(3):264–269
42. Wang Y, Jin K, Greenberg DA (2007) Neurogenesis associated with endothelin-induced cortical infarction in the mouse. Brain Res 1167:118–122
43. Tschirgi RD (1950) Protein complexes and the impermeability of the blood-brain barrier to dyes. Am J Physiol 163:756
44. Reynolds DS, Morton AJ (1998) Changes in blood-brain barrier permeability following neurotoxic lesions of rat brain can be visualised with trypan blue. J Neurosci Methods 79(1):115–121
45. Windle WF, Rhines R, Rankin J (1943) A Nissl method using buffered solutions of thionin. Stain Technol 18(2):77–86
46. Garcia-Cabezas MA, John YJ, Barbas H, Zikopoulos B (2016) Distinction of neurons, glia and endothelial cells in the cerebral cortex: an algorithm based on cytological features. Front Neuroanat 10:107
47. Popp A, Jaenisch N, Witte OW, Frahm C (2009) Identification of ischemic regions in a rat model of stroke. PLoS ONE 4(3):e4764
48. Sibatani A (1952) Differential staining of nucleic acids II. Cytologia 16(4):325–334
49. Ooigawa H, Nawashiro H, Fukui S, Otani N, Osumi A, Toyooka T, Shima K (2006) The fate of Nissl-stained dark neurons following traumatic brain injury in rats: difference between neocortex and hippocampus regarding survival rate. Acta Neuropathol 112(4):471–481
50. Ishida K, Shimizu H, Hida H, Urakawa S, Ida K, Nishino H (2004) Argyrophilic dark neurons represent various states of neuronal damage in brain insults: some come to die and others survive. Neuroscience 125(3):633–644
51. Benedek A, Móricz K, Jurányi Z, Gigler G, Lévay G, Hársing LG, Mátyus P, Szénási G, Albert M (2006) Use of TTC staining for the evaluation of tissue injury in the early phases of reperfusion after focal cerebral ischemia in rats. Brain Res 1116(1):159–165
52. Goldlust EJ, Paczynski RP, He YY, Hsu CY, Goldberg MP (1996) Automated measurement of infarct size with scanned images of triphenyltetrazolium chloride-stained rat brains. Stroke 27(9):1657–1662
53. Symon L (1987) Recovery of brain function after ischaemia. Acta Neurochir Suppl 41:97–103
54. Heiss WD (2010) The concept of the penumbra: can it be translated to stroke management? Int J Stroke 5(4):290–295
55. Meng X, Fisher M, Shen Q, Sotak CH, Duong TQ (2004) Characterizing the diffusion/perfusion mismatch in experimental focal cerebral ischemia. Ann Neurol 55(2):207–212
56. McCabe C, Gallagher L, Gsell W, Graham D, Dominiczak AF, Macrae IM (2009) Differences in the evolution of the ischemic penumbra in stroke-prone spontaneously hypertensive and Wistar-Kyoto rats. Stroke 40(12):3864–3868
57. Raghupathi R (2004) Cell death mechanisms following traumatic brain injury. Brain Pathol 14(2):215–222
58. Raghupathi R, Graham DI, McIntosh TK (2000) Apoptosis after traumatic brain injury. J Neurotrauma 17(10):927–938
59. Talanian RV, Quinlan C, Trautz S, Hackett MC, Mankovich JA, Banach D, Ghayur T, Brady KD, Wong WW (1997) Substrate specificities of caspase family proteases. J Biol Chem 272(15):9677–9682
60. Poreba M, Strozyk A, Salvesen GS, Drag M (2013) Caspase substrates and inhibitors. Cold Spring Harb Perspect Biol 5(8):a008680
61. Thornberry NA, Rano TA, Peterson EP, Rasper DM, Timkey T, Garcia-Calvo M, Houtzager VM, Nordstrom PA, Roy S, Vaillancourt JP, Chapman KT, Nicholson DW (1997) A combinatorial approach defines specificities of members of the caspase family and granzyme B. Functional relationships established for key mediators of apoptosis. J Biol Chem 272(29):17907–17911
62. Leenen PJ, de Bruijn MF, Voerman JS, Campbell PA, van Ewijk W (1994) Markers of mouse macrophage development detected by monoclonal antibodies. J Immunol Methods 174(1–2):5–19
63. Alliot F, Godin I, Pessac B (1999) Microglia derive from progenitors, originating from the yolk sac, and which proliferate in the brain. Brain Res Dev Brain Res 117(2):145–152
64. Prinz M, Priller J, Sisodia SS, Ransohoff RM (2011) Heterogeneity of CNS myeloid cells and their roles in neurodegeneration. Nat Neurosci 14:1227
65. Greter M, Lelios I, Croxford AL (2015) Microglia versus myeloid cell nomenclature during brain inflammation. Front Immunol 6:249
66. Jeong H-K, Ji K, Min K, Joe E-H (2013) Brain inflammation and microglia: facts and misconceptions. Exp Neurobiol 22(2):59–67
67. Vanni MP, Chan AW, Balbi M, Silasi G, Murphy TH (2017) Mesoscale mapping of mouse cortex reveals frequency-dependent cycling between distinct macroscale functional modules. J Neurosci 37(31):7513–7533